BABAR-CONF-04/42
SLAC-PUB-10634
hep-ex/0408073
August 2004

$B^0 \to K^+\pi^-\pi^0$ Dalitz Plot Analysis

The *BABAR* Collaboration

August 16, 2004

Abstract

We present preliminary results on the Dalitz plot analysis of $B^0 \to K^+\pi^-\pi^0$ decays. The data sample comprises 213 million $\Upsilon(4S) \to B\overline{B}$ decays collected with the *BABAR* detector at the PEP-II asymmetric-energy B Factory at SLAC. We report measurements of the inclusive branching fraction, quasi-two-body fractions and *CP*-violating charge asymmetries for intermediate states including $K^*(892)^+\pi^-$ and $\rho(770)^-K^+$. Observations of B^0 decays to the $K\pi$ S-wave intermediate states, $K_0^*(1430)^+\pi^-$ and $K_0^*(1430)^0\pi^0$, are reported. Evidence of the decay $B^0 \to K^*(892)^0\pi^0$ is seen. We set upper limits at 90% confidence level on branching fractions of the nonresonant and other less significant intermediate states.

Submitted to the 32nd International Conference on High-Energy Physics, ICHEP 04,
16 August—22 August 2004, Beijing, China

Stanford Linear Accelerator Center, Stanford University, Stanford, CA 94309

Work supported in part by Department of Energy contract DE-AC03-76SF00515.

The *BABAR* Collaboration,

B. Aubert, R. Barate, D. Boutigny, F. Couderc, J.-M. Gaillard, A. Hicheur, Y. Karyotakis, J. P. Lees, V. Tisserand, A. Zghiche

Laboratoire de Physique des Particules, F-74941 Annecy-le-Vieux, France

A. Palano, A. Pompili

Università di Bari, Dipartimento di Fisica and INFN, I-70126 Bari, Italy

J. C. Chen, N. D. Qi, G. Rong, P. Wang, Y. S. Zhu

Institute of High Energy Physics, Beijing 100039, China

G. Eigen, I. Ofte, B. Stugu

University of Bergen, Inst. of Physics, N-5007 Bergen, Norway

G. S. Abrams, A. W. Borgland, A. B. Breon, D. N. Brown, J. Button-Shafer, R. N. Cahn, E. Charles, C. T. Day, M. S. Gill, A. V. Gritsan, Y. Groysman, R. G. Jacobsen, R. W. Kadel, J. Kadyk, L. T. Kerth, Yu. G. Kolomensky, G. Kukartsev, G. Lynch, L. M. Mir, P. J. Oddone, T. J. Orimoto, M. Pripstein, N. A. Roe, M. T. Ronan, V. G. Shelkov, W. A. Wenzel

Lawrence Berkeley National Laboratory and University of California, Berkeley, CA 94720, USA

M. Barrett, K. E. Ford, T. J. Harrison, A. J. Hart, C. M. Hawkes, S. E. Morgan, A. T. Watson

University of Birmingham, Birmingham, B15 2TT, United Kingdom

M. Fritsch, K. Goetzen, T. Held, H. Koch, B. Lewandowski, M. Pelizaeus, M. Steinke

Ruhr Universität Bochum, Institut für Experimentalphysik 1, D-44780 Bochum, Germany

J. T. Boyd, N. Chevalier, W. N. Cottingham, M. P. Kelly, T. E. Latham, F. F. Wilson

University of Bristol, Bristol BS8 1TL, United Kingdom

T. Cuhadar-Donszelmann, C. Hearty, N. S. Knecht, T. S. Mattison, J. A. McKenna, D. Thiessen

University of British Columbia, Vancouver, BC, Canada V6T 1Z1

A. Khan, P. Kyberd, L. Teodorescu

Brunel University, Uxbridge, Middlesex UB8 3PH, United Kingdom

A. E. Blinov, V. E. Blinov, V. P. Druzhinin, V. B. Golubev, V. N. Ivanchenko, E. A. Kravchenko, A. P. Onuchin, S. I. Serednyakov, Yu. I. Skovpen, E. P. Solodov, A. N. Yushkov

Budker Institute of Nuclear Physics, Novosibirsk 630090, Russia

D. Best, M. Bruinsma, M. Chao, I. Eschrich, D. Kirkby, A. J. Lankford, M. Mandelkern, R. K. Mommsen, W. Roethel, D. P. Stoker

University of California at Irvine, Irvine, CA 92697, USA

C. Buchanan, B. L. Hartfiel

University of California at Los Angeles, Los Angeles, CA 90024, USA

S. D. Foulkes, J. W. Gary, B. C. Shen, K. Wang

University of California at Riverside, Riverside, CA 92521, USA

D. del Re, H. K. Hadavand, E. J. Hill, D. B. MacFarlane, H. P. Paar, Sh. Rahatlou, V. Sharma

University of California at San Diego, La Jolla, CA 92093, USA

J. W. Berryhill, C. Campagnari, B. Dahmes, O. Long, A. Lu, M. A. Mazur, J. D. Richman, W. Verkerke

University of California at Santa Barbara, Santa Barbara, CA 93106, USA

T. W. Beck, A. M. Eisner, C. A. Heusch, J. Kroseberg, W. S. Lockman, G. Nesom, T. Schalk, B. A. Schumm, A. Seiden, P. Spradlin, D. C. Williams, M. G. Wilson

University of California at Santa Cruz, Institute for Particle Physics, Santa Cruz, CA 95064, USA

J. Albert, E. Chen, G. P. Dubois-Felsmann, A. Dvoretskii, D. G. Hitlin, I. Narsky, T. Piatenko, F. C. Porter, A. Ryd, A. Samuel, S. Yang

California Institute of Technology, Pasadena, CA 91125, USA

S. Jayatilleke, G. Mancinelli, B. T. Meadows, M. D. Sokoloff

University of Cincinnati, Cincinnati, OH 45221, USA

T. Abe, F. Blanc, P. Bloom, S. Chen, W. T. Ford, U. Nauenberg, A. Olivas, P. Rankin, J. G. Smith, J. Zhang, L. Zhang

University of Colorado, Boulder, CO 80309, USA

A. Chen, J. L. Harton, A. Soffer, W. H. Toki, R. J. Wilson, Q. Zeng

Colorado State University, Fort Collins, CO 80523, USA

D. Altenburg, T. Brandt, J. Brose, M. Dickopp, E. Feltresi, A. Hauke, H. M. Lacker, R. Müller-Pfefferkorn, R. Nogowski, S. Otto, A. Petzold, J. Schubert, K. R. Schubert, R. Schwierz, B. Spaan, J. E. Sundermann

Technische Universität Dresden, Institut für Kern- und Teilchenphysik, D-01062 Dresden, Germany

D. Bernard, G. R. Bonneaud, F. Brochard, P. Grenier, S. Schrenk, Ch. Thiebaux, G. Vasileiadis, M. Verderi

Ecole Polytechnique, LLR, F-91128 Palaiseau, France

D. J. Bard, P. J. Clark, D. Lavin, F. Muheim, S. Playfer, Y. Xie

University of Edinburgh, Edinburgh EH9 3JZ, United Kingdom

M. Andreotti, V. Azzolini, D. Bettoni, C. Bozzi, R. Calabrese, G. Cibinetto, E. Luppi, M. Negrini, L. Piemontese, A. Sarti

Università di Ferrara, Dipartimento di Fisica and INFN, I-44100 Ferrara, Italy

E. Treadwell

Florida A&M University, Tallahassee, FL 32307, USA

F. Anulli, R. Baldini-Ferroli, A. Calcaterra, R. de Sangro, G. Finocchiaro, P. Patteri, I. M. Peruzzi, M. Piccolo, A. Zallo

Laboratori Nazionali di Frascati dell'INFN, I-00044 Frascati, Italy

A. Buzzo, R. Capra, R. Contri, G. Crosetti, M. Lo Vetere, M. Macri, M. R. Monge, S. Passaggio, C. Patrignani, E. Robutti, A. Santroni, S. Tosi

Università di Genova, Dipartimento di Fisica and INFN, I-16146 Genova, Italy

S. Bailey, G. Brandenburg, K. S. Chaisanguanthum, M. Morii, E. Won

Harvard University, Cambridge, MA 02138, USA

R. S. Dubitzky, U. Langenegger

Universität Heidelberg, Physikalisches Institut, Philosophenweg 12, D-69120 Heidelberg, Germany

W. Bhimji, D. A. Bowerman, P. D. Dauncey, U. Egede, J. R. Gaillard, G. W. Morton, J. A. Nash, M. B. Nikolich, G. P. Taylor

Imperial College London, London, SW7 2AZ, United Kingdom

M. J. Charles, G. J. Grenier, U. Mallik

University of Iowa, Iowa City, IA 52242, USA

J. Cochran, H. B. Crawley, J. Lamsa, W. T. Meyer, S. Prell, E. I. Rosenberg, A. E. Rubin, J. Yi

Iowa State University, Ames, IA 50011-3160, USA

M. Biasini, R. Covarelli, M. Pioppi

Università di Perugia, Dipartimento di Fisica and INFN, I-06100 Perugia, Italy

M. Davier, X. Giroux, G. Grosdidier, A. Höcker, S. Laplace, F. Le Diberder, V. Lepeltier, A. M. Lutz, T. C. Petersen, S. Plaszczynski, M. H. Schune, L. Tantot, G. Wormser

Laboratoire de l'Accélérateur Linéaire, F-91898 Orsay, France

C. H. Cheng, D. J. Lange, M. C. Simani, D. M. Wright

Lawrence Livermore National Laboratory, Livermore, CA 94550, USA

A. J. Bevan, C. A. Chavez, J. P. Coleman, I. J. Forster, J. R. Fry, E. Gabathuler, R. Gamet, D. E. Hutchcroft, R. J. Parry, D. J. Payne, R. J. Sloane, C. Touramanis

University of Liverpool, Liverpool L69 72E, United Kingdom

J. J. Back,[1] C. M. Cormack, P. F. Harrison,[1] F. Di Lodovico, G. B. Mohanty[1]

Queen Mary, University of London, E1 4NS, United Kingdom

C. L. Brown, G. Cowan, R. L. Flack, H. U. Flaecher, M. G. Green, P. S. Jackson, T. R. McMahon, S. Ricciardi, F. Salvatore, M. A. Winter

University of London, Royal Holloway and Bedford New College, Egham, Surrey TW20 0EX, United Kingdom

D. Brown, C. L. Davis

University of Louisville, Louisville, KY 40292, USA

J. Allison, N. R. Barlow, R. J. Barlow, P. A. Hart, M. C. Hodgkinson, G. D. Lafferty, A. J. Lyon, J. C. Williams

University of Manchester, Manchester M13 9PL, United Kingdom

A. Farbin, W. D. Hulsbergen, A. Jawahery, D. Kovalskyi, C. K. Lae, V. Lillard, D. A. Roberts

University of Maryland, College Park, MD 20742, USA

G. Blaylock, C. Dallapiccola, K. T. Flood, S. S. Hertzbach, R. Kofler, V. B. Koptchev, T. B. Moore, S. Saremi, H. Staengle, S. Willocq

University of Massachusetts, Amherst, MA 01003, USA

[1]Now at Department of Physics, University of Warwick, Coventry, United Kingdom

R. Cowan, G. Sciolla, S. J. Sekula, F. Taylor, R. K. Yamamoto

Massachusetts Institute of Technology, Laboratory for Nuclear Science, Cambridge, MA 02139, USA

D. J. J. Mangeol, P. M. Patel, S. H. Robertson

McGill University, Montréal, QC, Canada H3A 2T8

A. Lazzaro, V. Lombardo, F. Palombo

Università di Milano, Dipartimento di Fisica and INFN, I-20133 Milano, Italy

J. M. Bauer, L. Cremaldi, V. Eschenburg, R. Godang, R. Kroeger, J. Reidy, D. A. Sanders, D. J. Summers, H. W. Zhao

University of Mississippi, University, MS 38677, USA

S. Brunet, D. Côté, P. Taras

Université de Montréal, Laboratoire René J. A. Lévesque, Montréal, QC, Canada H3C 3J7

H. Nicholson

Mount Holyoke College, South Hadley, MA 01075, USA

N. Cavallo,[2] F. Fabozzi,[2] C. Gatto, L. Lista, D. Monorchio, P. Paolucci, D. Piccolo, C. Sciacca

Università di Napoli Federico II, Dipartimento di Scienze Fisiche and INFN, I-80126, Napoli, Italy

M. Baak, H. Bulten, G. Raven, H. L. Snoek, L. Wilden

NIKHEF, National Institute for Nuclear Physics and High Energy Physics, NL-1009 DB Amsterdam, The Netherlands

C. P. Jessop, J. M. LoSecco

University of Notre Dame, Notre Dame, IN 46556, USA

T. Allmendinger, K. K. Gan, K. Honscheid, D. Hufnagel, H. Kagan, R. Kass, T. Pulliam, A. M. Rahimi, R. Ter-Antonyan, Q. K. Wong

Ohio State University, Columbus, OH 43210, USA

J. Brau, R. Frey, O. Igonkina, C. T. Potter, N. B. Sinev, D. Strom, E. Torrence

University of Oregon, Eugene, OR 97403, USA

F. Colecchia, A. Dorigo, F. Galeazzi, M. Margoni, M. Morandin, M. Posocco, M. Rotondo, F. Simonetto, R. Stroili, G. Tiozzo, C. Voci

Università di Padova, Dipartimento di Fisica and INFN, I-35131 Padova, Italy

M. Benayoun, H. Briand, J. Chauveau, P. David, Ch. de la Vaissière, L. Del Buono, O. Hamon, M. J. J. John, Ph. Leruste, J. Malcles, J. Ocariz, M. Pivk, L. Roos, S. T'Jampens, G. Therin

Universités Paris VI et VII, Laboratoire de Physique Nucléaire et de Hautes Energies, F-75252 Paris, France

P. F. Manfredi, V. Re

Università di Pavia, Dipartimento di Elettronica and INFN, I-27100 Pavia, Italy

[2]Also with Università della Basilicata, Potenza, Italy

P. K. Behera, L. Gladney, Q. H. Guo, J. Panetta

University of Pennsylvania, Philadelphia, PA 19104, USA

C. Angelini, G. Batignani, S. Bettarini, M. Bondioli, F. Bucci, G. Calderini, M. Carpinelli, F. Forti, M. A. Giorgi, A. Lusiani, G. Marchiori, F. Martinez-Vidal,[3] M. Morganti, N. Neri, E. Paoloni, M. Rama, G. Rizzo, F. Sandrelli, J. Walsh

Università di Pisa, Dipartimento di Fisica, Scuola Normale Superiore and INFN, I-56127 Pisa, Italy

M. Haire, D. Judd, K. Paick, D. E. Wagoner

Prairie View A&M University, Prairie View, TX 77446, USA

N. Danielson, P. Elmer, Y. P. Lau, C. Lu, V. Miftakov, J. Olsen, A. J. S. Smith, A. V. Telnov

Princeton University, Princeton, NJ 08544, USA

F. Bellini, G. Cavoto,[4] R. Faccini, F. Ferrarotto, F. Ferroni, M. Gaspero, L. Li Gioi, M. A. Mazzoni, S. Morganti, M. Pierini, G. Piredda, F. Safai Tehrani, C. Voena

Università di Roma La Sapienza, Dipartimento di Fisica and INFN, I-00185 Roma, Italy

S. Christ, G. Wagner, R. Waldi

Universität Rostock, D-18051 Rostock, Germany

T. Adye, N. De Groot, B. Franek, N. I. Geddes, G. P. Gopal, E. O. Olaiya

Rutherford Appleton Laboratory, Chilton, Didcot, Oxon, OX11 0QX, United Kingdom

R. Aleksan, S. Emery, A. Gaidot, S. F. Ganzhur, P.-F. Giraud, G. Hamel de Monchenault, W. Kozanecki, M. Legendre, G. W. London, B. Mayer, G. Schott, G. Vasseur, Ch. Yèche, M. Zito

DSM/Dapnia, CEA/Saclay, F-91191 Gif-sur-Yvette, France

M. V. Purohit, A. W. Weidemann, J. R. Wilson, F. X. Yumiceva

University of South Carolina, Columbia, SC 29208, USA

D. Aston, R. Bartoldus, N. Berger, A. M. Boyarski, O. L. Buchmueller, R. Claus, M. R. Convery, M. Cristinziani, G. De Nardo, D. Dong, J. Dorfan, D. Dujmic, W. Dunwoodie, E. E. Elsen, S. Fan, R. C. Field, T. Glanzman, S. J. Gowdy, T. Hadig, V. Halyo, C. Hast, T. Hryn'ova, W. R. Innes, M. H. Kelsey, P. Kim, M. L. Kocian, D. W. G. S. Leith, J. Libby, S. Luitz, V. Luth, H. L. Lynch, H. Marsiske, R. Messner, D. R. Muller, C. P. O'Grady, V. E. Ozcan, A. Perazzo, M. Perl, S. Petrak, B. N. Ratcliff, A. Roodman, A. A. Salnikov, R. H. Schindler, J. Schwiening, G. Simi, A. Snyder, A. Soha, J. Stelzer, D. Su, M. K. Sullivan, J. Va'vra, S. R. Wagner, M. Weaver, A. J. R. Weinstein, W. J. Wisniewski, M. Wittgen, D. H. Wright, A. K. Yarritu, C. C. Young

Stanford Linear Accelerator Center, Stanford, CA 94309, USA

P. R. Burchat, A. J. Edwards, T. I. Meyer, B. A. Petersen, C. Roat

Stanford University, Stanford, CA 94305-4060, USA

S. Ahmed, M. S. Alam, J. A. Ernst, M. A. Saeed, M. Saleem, F. R. Wappler

State University of New York, Albany, NY 12222, USA

[3]Also with IFIC, Instituto de Física Corpuscular, CSIC-Universidad de Valencia, Valencia, Spain
[4]Also with Princeton University, Princeton, USA

W. Bugg, M. Krishnamurthy, S. M. Spanier
University of Tennessee, Knoxville, TN 37996, USA

R. Eckmann, H. Kim, J. L. Ritchie, A. Satpathy, R. F. Schwitters
University of Texas at Austin, Austin, TX 78712, USA

J. M. Izen, I. Kitayama, X. C. Lou, S. Ye
University of Texas at Dallas, Richardson, TX 75083, USA

F. Bianchi, M. Bona, F. Gallo, D. Gamba
Università di Torino, Dipartimento di Fisica Sperimentale and INFN, I-10125 Torino, Italy

L. Bosisio, C. Cartaro, F. Cossutti, G. Della Ricca, S. Dittongo, S. Grancagnolo, L. Lanceri, P. Poropat,[5] L. Vitale, G. Vuagnin
Università di Trieste, Dipartimento di Fisica and INFN, I-34127 Trieste, Italy

R. S. Panvini
Vanderbilt University, Nashville, TN 37235, USA

Sw. Banerjee, C. M. Brown, D. Fortin, P. D. Jackson, R. Kowalewski, J. M. Roney, R. J. Sobie
University of Victoria, Victoria, BC, Canada V8W 3P6

H. R. Band, B. Cheng, S. Dasu, M. Datta, A. M. Eichenbaum, M. Graham, J. J. Hollar, J. R. Johnson, P. E. Kutter, H. Li, R. Liu, A. Mihalyi, A. K. Mohapatra, Y. Pan, R. Prepost, P. Tan, J. H. von Wimmersperg-Toeller, J. Wu, S. L. Wu, Z. Yu
University of Wisconsin, Madison, WI 53706, USA

M. G. Greene, H. Neal
Yale University, New Haven, CT 06511, USA

[5]Deceased

1 INTRODUCTION

Charmless three-body B decays significantly broaden the understanding of B meson decay mechanisms and provide additional possibilities for direct CP violation searches. The $B^0 \to K^+\pi^-\pi^0$ decay is known to have contributions from the charmless intermediate $B^0 \to K^*(892)^+\pi^-$ and $B^0 \to \rho(770)^-K^+$ decays. Although not yet observed, $B^0 \to K^*(892)^0\pi^0$ could also contribute, as well as $K_0^*(1430)$, $K_2^*(1430)$, $K^*(1680)$, $\rho(1450)$, and $\rho(1700)$. The $B^0 \to K^+\pi^-\pi^0$ decay can also occur via long-lived charmed intermediate states, *i.e.*, $B^0 \to \overline{D}^0\pi^0$, and the doubly-Cabibbo-suppressed $B^0 \to D^-K^+$, $D^- \to \pi^-\pi^0$. Intermediate states with broad resonances are interfering and therefore a full amplitude analysis is required to extract the amplitudes and relative phases. Quasi-two-body branching fractions and CP-violating charge asymmetries for intermediate states are also measured. The results can be used to probe the weak phase $\gamma \equiv \arg\left[-V_{ud}V_{ub}^*/V_{cd}V_{cb}^*\right]$ of the Unitarity Triangle [1, 2].

The charmless intermediate states are largely dominated by a gluonic penguin diagram ($\bar{b} \to u\bar{u}\bar{s}$ or $d\bar{d}\bar{s}$), while the electroweak penguin contribution may also be sizeable [3]. The Dalitz plot analysis provides a sensitive probe on the penguin contributions to B decays to a charmless vector meson and a charmless pseudoscalar meson.

Measurements of some of the branching fractions and charge asymmetries have been carried out by CLEO [4], *BABAR* [5] and Belle [6] in the quasi-two-body approximation. In this report, we present a Dalitz plot analysis that takes into account interference between individual modes, using a Maximum Likelihood (ML) approach. Unless stated otherwise, charge conjugation is always implied throughout this paper.

2 THE *BABAR* DETECTOR AND DATASET

The data used in this analysis were collected with the *BABAR* detector at the PEP-II asymmetric-energy e^+e^- storage ring. The sample consists of 213 million $B\overline{B}$ pairs, corresponding to an integrated luminosity of 193.2 fb^{-1} collected at the $\Upsilon(4S)$ resonance ("on-resonance"), and an integrated luminosity of 16 fb^{-1} collected about 40 MeV below the $\Upsilon(4S)$ ("off-resonance").

The *BABAR* detector is described in detail elsewhere [7]. A five-layer double-sided silicon vertex tracker (SVT) and a 40-layer drift chamber (DCH) are used to detect charged particles and measure their momentum as well as ionization energy loss (dE/dx). Charged hadrons are identified with a detector of internally reflected Cherenkov light (DIRC) and ionization in the tracking detectors. Photons, neutral hadrons, and electrons are detected in a CsI(Tl) calorimeter (EMC), while muons are identified in the magnetic flux return system (IFR).

3 ANALYSIS METHOD

3.1 Event Selection

Each signal B candidate is reconstructed from K^+, π^-, and π^0 candidates. Charged tracks must have at least 12 hits in the DCH and a transverse momentum larger than 100 MeV/c. Charged tracks identified as electrons, muons or protons are rejected. We also require that the charged kaon candidate must be identified as a kaon and that the charged pion candidate must not be identified as a kaon. The π^0 candidate must have a mass that satisfies $0.11 < m(\gamma\gamma) < 0.16\,\mathrm{GeV}/c^2$, and each

photon is required to have an energy greater than 50 MeV in the laboratory frame and to exhibit a lateral profile of energy deposition in the EMC consistent with an electromagnetic shower.

Two kinematic variables, ΔE and $m_{\rm ES}$, allow the discrimination of signal B decays from random combinations of tracks and π^0 candidates. The energy difference, ΔE, is the difference between the e^+e^- center-of-mass (CM) energy of the B candidate and $\sqrt{s}/2$, where $\sqrt{s}$ is the total CM energy. The beam-energy-substituted mass, $m_{\rm ES}$, is defined by $\sqrt{(s/2+\mathbf{p}_i\cdot\mathbf{p}_B)^2/E_i^2-\mathbf{p}_B^2}$, where the B momentum, $\mathbf{p}_B$, and the four-momentum of the initial e^+e^- state (E_i, $\mathbf{p}_i$) are measured in the laboratory frame. For the signal B candidate, we require that $m_{\rm ES} > 5.27\,{\rm GeV}/c^2$. The ΔE resolution depends on the π^0 energy and therefore varies across the Dalitz plot. To account for this effect, we introduce a transformed quantity:

$$\Delta E' \equiv \frac{2\Delta E - (\Delta E_{max} + \Delta E_{min})}{\Delta E_{max} - \Delta E_{min}}\,, \tag{1}$$

where $\Delta E_{max} = 0.08 - 0.0014\cdot m(K^+\pi^-)$, $\Delta E_{min} = -0.14 + 0.0038\cdot m(K^+\pi^-)$, all in units of GeV. We require $|\Delta E'| \leq 1$.

Continuum $e^+e^- \to q\bar{q}$ ($q = u, d, s, c$) events are the dominant background. To enhance discrimination between signal and continuum, we utilize a neural network (NN) which combines four discriminating variables: the cosine of the angle between the B momentum and the e^+ beam direction in the CM frame, the cosine of the angle between the B thrust axis and the beam direction in the CM frame, and two event-shape variables defined as sums over all particles i of $p_i \times |\cos\theta_i|^n$, where $n = 0$ or 2, and θ_i is the angle between the momentum of particle i and the B thrust axis. The NN weights the discriminating variables differently, according to training on off-resonance data and simulated signal events. We cut on the NN output to suppress about 95% of the continuum background while retaining 62% of the signal.

The fraction of events that have more than one candidate satisfying the selection depends on the kinematical distributions of the B decay products, and is therefore different for each mode. When more than one π^0 candidate is present in the event, we choose the candidate with the reconstructed π^0 mass closest to the nominal value of 0.1349 GeV/c^2. If more than one charged track combination satisfies the selection, we randomly choose one B candidate. An event is classified as misreconstructed signal if it contains a B which decays to the signal mode, but one or more reconstructed particles are not actually from the decay of that B. Misreconstructed signal is called self cross feed (SCF). This misreconstruction is primarily due to the presence of low momentum pions in the B decays and thus the SCF fraction varies across the Dalitz plot.

There are 7220 events selected from the data sample. Table 1 summarizes the signal efficiencies (including the misreconstructed events) and the misreconstruction fractions (with respect to the total signal) estimated from simulation with non-interfering amplitudes.

We use simulated events to study the background from other B decays (B-background) which includes both charmed ($b \to c$) and charmless decays. In the selected $B^0 \to K^+\pi^-\pi^0$ sample we expect 503 ± 151 $b \to c$ background events. The decays $B^0 \to \overline{D}^0\pi^0, \overline{D}^0 \to K^+\pi^-$ and $B^0 \to D^-K^+, D^- \to \pi^-\pi^0$ have the same final state as the charmless intermediate states of our interest, but they do not interfer with the charmless intermediate states. Both are technically treated as B-backgrounds, but separately from other charmed background events. Branching fractions of $B^0 \to \overline{D}^0\pi^0$ and $B^0 \to D^-K^+$ have been already measured, albeit with large uncertainties. In the present analysis, while we still do not have enough sensitivity to observe the doubly-Cabibbo suppressed $B^0 \to D^-K^+$, $D^- \to \pi^-\pi^0$, we measure the branching fraction of the $B^0 \to \overline{D}^0\pi^0$ decay. The selection efficiency for this mode is $(16.7 \pm 0.1)\%$ with a misreconstruction fraction of

Table 1: Signal efficiencies (misreconstructed events (SCF) included), fractions of misreconstructed events, for the different intermediate signal modes. The errors given are statistical only.

Decay mode	$\varepsilon(\%)$	$f_{\rm SCF}(\%)$
$K^*(892)^+\pi^-$	14.9 ± 0.1	23.6 ± 0.3
$\rho^- K^+$	16.7 ± 0.0	22.2 ± 0.1
$K^*(892)^0\pi^0$	16.8 ± 0.1	8.7 ± 0.2
$nonresonant$	16.3 ± 0.0	3.8 ± 0.0
$K_0^*(1430)^+\pi^-$	15.5 ± 0.1	9.0 ± 0.2
$K_0^*(1430)^0\pi^0$	17.4 ± 0.1	4.2 ± 0.2

$(2.6 \pm 0.1)\%$. We expect 230 ± 20 charmless B-background events in the data sample. The major charmless B-background modes include $B^0 \to K^*(892)^0\gamma$, $K^*(1430)^0\gamma$, $B^0 \to K^+\pi^-$, $B^+ \to K^+\pi^0$, $B^0 \to \rho^+\pi^-$, $B^0 \to \rho^+\rho^-$, and $B^+ \to \rho^+\rho^0$. Other contributing modes include $B^+ \to K^*(892)^+\pi^0$, $B^+ \to f^0K^+$, $B^+ \to K_0^*(1430)^0\pi^+$, and $B^+ \to \eta' K^+$. The branching fractions of unmeasured decay channels are estimated within conservative error ranges. Charmless B-background modes are grouped into six classes with similar kinematic and topological properties. Two additional classes account for the inclusive neutral and charged $b \to c$ decays. In total, ten classes for B backgrounds are defined.

3.2 Dalitz Plot

For the decay $B^0 \to K^+\pi^-\pi^0$, with four momentum p_{B^0}, p_+, p_- and p_0 respectively, the differential decay width with respect to the invariant-mass-squared variables (*i.e.*, the *Dalitz plot variables* (DP)) reads

$$d\Gamma(B^0 \to K^+\pi^-\pi^0) \;=\; \frac{1}{(2\pi)^3}\frac{|\mathcal{A}_{B^0\to K^+\pi^-\pi^0}|^2}{8m_{B^0}^3}\, ds_{+-}ds_{-0}\;, \tag{2}$$

where $\mathcal{A}_{B^0\to K^+\pi^-\pi^0}$ is the Lorentz-invariant amplitude of the three-body decay and

$$s_{+-} \;=\; (p_+ + p_-)^2\;, \qquad s_{-0} \;=\; (p_- + p_0)^2\;. \tag{3}$$

The amplitude $\mathcal{A}_{B^0\to K^+\pi^-\pi^0}$ contains all the underlying dynamics of the $B^0 \to K^+\pi^-\pi^0$ decay. In general, it is the coherent sum of one nonresonant (NR) term, $\mathcal{A}_{\rm NR}$, which is assumed to be constant in the Dalitz plane, and of several resonant amplitudes, i, having spin J, magnitude a_i, and phase ϕ_i:

$$\mathcal{A}_{B^0\to K^+\pi^-\pi^0}(s_{+-}\,, s_{-0}) \;=\; a_{\rm NR}e^{i\phi_{\rm NR}}\mathcal{A}_{\rm NR} \;+\sum_i a_i e^{i\phi_i}\cdot\mathcal{A}_i(s_{+-}\,, s_{-0})\;. \tag{4}$$

A similar expression is implied for $\overline{B^0}$ decays, with $\overline{a}_{\rm NR}$, $\overline{\phi}_{\rm NR}$, $\overline{a}_i$, and $\overline{\phi}_i$ being assumed different from $a_{\rm NR}$, $\phi_{\rm NR}$, a_i, and ϕ_i, respectively.

The resonant amplitude $\mathcal{A}_i$ is written as a product of four terms

$$\mathcal{A}_i(\mathrm{DP}) \;\;=\;\; {}^JF_{B,i}\cdot{}^JF_i(s)\cdot{}^JK(\mathrm{DP})\cdot{}^JF_{R,i}(s)\;, \tag{5}$$

where ${}^JF_{B,i}$ is an irrelevant constant form factor for the B^0 decay and is absorbed by normalization, ${}^JF_i(s) \equiv {}^JF(Rq(s))/{}^JF(Rq(m_i^2))$ is the ratio of Blatt-Weisskopf damping factors (see below),

${}^{J}K(\mathrm{DP})$ is a kinematic function (see below), and ${}^{J}F_{R,i}(s)$ is a dynamic function describing the resonance (see below).

For a resonance decays to particles a and b, with invariant mass $\sqrt{s}$, the momentum of the particles a and b in the resonance rest frame, q, is given by

$$q(s) \;=\; \frac{\sqrt{s}}{2}\left(1-\frac{(m_a+m_b)^2}{s}\right)^{1/2}\left(1-\frac{(m_a-m_b)^2}{s}\right)^{1/2} \quad , \tag{6}$$

where m_a and m_b are the masses of particle a and b, respectively.

The functions ${}^{J}F(Rq(s))$ are the nuclear *Blatt-Weisskopf damping factors* [8], given by

$${}^{0}F \;=\; 1\;, \quad {}^{1}F \;=\; \frac{1}{\sqrt{1+R^2q^2}}\;, \quad {}^{2}F \;=\; \frac{1}{\sqrt{9+3R^2q^2+R^4q^4}}\;, \tag{7}$$

where R is the range parameter. The Blatt-Weisskopf damping factors are studied only for systematic uncertainty evaluation.

The spin-dependent function is taken to be equal to 1 for a spin-0 resonance, $-2|\mathbf{p_d}||\mathbf{p_b}|\cos\theta$ for spin-1, and $\frac{4}{3}(|\mathbf{p_d}||\mathbf{p_b}|)^2(3\cos^2\theta-1)$ for spin-2, where $\mathbf{p_d}$ is the three-momentum of one of the resonance daughters and $\mathbf{p_b}$ is the three-momentum of the bachelor particle, both measured in the resonance rest frame, and θ is the helicity angle of the resonance. For a resonance formed from $K^+\pi^0$ ($\pi^-\pi^0$), the helicity angle is defined by the angle between the π^0 (π^-) in the resonance rest frame and the resonance flight direction in the B^0 rest frame. For a resonance formed from $K^+\pi^-$, the helicity angle is defined by the angle between the K^+ in the resonance rest frame and the resonance flight direction in the B^0 rest frame.

Three parameterizations are considered to describe the decay dynamics, ${}^{J}F_{R,i}(s)$. Parameters are taken from [9] unless stated otherwise. The relativistic Breit-Wigner parameterization with mass-dependent width is used for $K^*(892)^{+,0}$, $K_2^*(1430)^{+,0}$, and $K^*(1680)^{+,0}$. It is given by

$${}^{J}F_{R,i}(s) \;=\; \frac{1}{s-m_i^2+im_i{}^{J}\Gamma_i(s)}\;. \tag{8}$$

The s-dependent width is defined by

$${}^{J}\Gamma_i(s) \;=\; \Gamma_i^0\frac{m_i}{\sqrt{s}}\left(\frac{q(s)}{q(m_i^2)}\right)^{2J+1}\frac{{}^{J}F^2(Rq(s))}{{}^{J}F^2(Rq(m_i^2))}\;, \tag{9}$$

where m_i is the mass of the resonance i, $\Gamma_i^0=\Gamma_i(m_i^2)$ its width.

The Gounaris-Sakurai parameterization [10] is used to parameterize $\rho(770)^-$, $\rho(1450)^-$ and $\rho(1700)^-$. For the $K\pi$ S-wave resonances, $K_0^*(1430)^{+,0}$, which are found to be dominant in the $K\pi$ invariant mass range below 2 GeV/c^2, an effective-range parameterization was suggested [11] to describe the slowly increasing phase as a function of $K\pi$ mass. We use the parameterization as used in the LASS experiment [12], being modified for B decays:

$$F_{R,i}^{LASS}(s) = \frac{\sqrt{s}}{q(s)\,\cot\delta_B - i\,q(s)} + e^{2i\delta_B}\,\frac{m_i^2\,\Gamma_i^0/q(m_i^2)}{m_i^2-s-i\,m_i\Gamma_i(s)}\,, \tag{10}$$

where

$$\cot\delta_B = \frac{1}{aq(s)}+\frac{1}{2}\,r\,q^2(s)\,, \tag{11}$$

$m_i = 1415 \pm 3\,\mathrm{MeV}/c^2$, $\Gamma_i^0 = 300 \pm 6\,\mathrm{MeV}/c^2$, the scattering length $a = 2.07 \pm 0.10\ (\mathrm{GeV}/c)^{-1}$, and the effective range $r = 3.32 \pm 0.34\ (\mathrm{GeV}/c)^{-2}$. Our results for $K_0^*(1430)$ reported in this paper are not purely due to the resonant term, but to the $K\pi$ S-wave as a whole.

Our nominal model includes the nonresonant contribution and five resonant intermediate states: $\rho(770)^-$, $K^*(892)^{+,0}$ and $K_0^*(1430)^{+,0}$. Variations to this nominal model are used to estimate the model-dependent systematic uncertainty in the results.

The quasi-two-body fractions and CP-violation charge asymmetries are extracted as follows:

$$f_i = \frac{\int (\,|a_i e^{i\phi_i}\mathcal{A}_i|^2 + |\overline{a}_i e^{i\overline{\phi}_i}\mathcal{A}_i|^2\,)\,ds_{+-}ds_{-0}}{\int (\,|\mathcal{A}_{B^0\to K^+\pi^-\pi^0}|^2 + |\overline{\mathcal{A}}_{\overline{B}^0\to K^-\pi^+\pi^0}|^2\,)\,ds_{+-}ds_{-0}}\,, \tag{12}$$

$$A_{\mathrm{CP}}^i = \frac{|\overline{a}_i|^2 - |a_i|^2}{|\overline{a}_i|^2 + |a_i|^2}\,, \tag{13}$$

where a_i and $\overline{a_i}$ are the fitted magnitudes, ϕ_i and $\overline{\phi}_i$ are the fitted relative phases, for the intermediate state i. The extraction is also valid for the nonresonant. Due to interference, the sum of the fractions will in general not add up to unity.

The inclusive branching fraction, $\mathcal{B}^{incl.}$, and the quasi-two-body branching fraction for an intermediate state i, $\mathcal{B}_i$, are given by:

$$\mathcal{B}^{incl.} = \frac{N_{sig}}{\overline{\varepsilon} N_{B\overline{B}}}\,, \quad \mathcal{B}_i = f_i \cdot \mathcal{B}^{incl.}\,, \tag{14}$$

where N_{sig} is the total signal observed in the data, $\overline{\varepsilon}$ is the signal efficiency averaged over the Dalitz plot, $N_{B\overline{B}}$ is the total number of $B\overline{B}$ pairs produced, and f_i is the fitted fraction for the intermediate state i, respectively.

3.3 Maximum Likelihood Fit

The selected on-resonance data sample is assumed to consist of signal, continuum-background and B-background components. We use the variables m_{ES}, $\Delta E'$, and the Dalitz plot to discriminate signal from background. The signal probability density function (PDF) contains two parts corresponding respectively to signal events that are correctly reconstructed (TM) and signal events that are misreconstructed (SCF). A PDF is introduced to describe the dominant continuum background. For B-related backgrounds, we study the contributions with exclusive simulations and group similar contributions into the 10 B background classes, each of which has an individual PDF in the fit.

The likelihood $\mathcal{L}$ for N events reads as

$$\begin{aligned}
\mathcal{L} = {} & e^{-N'} \prod_{i=1}^{N} \Big\{ N_{sig} \left[(1 - \overline{f}_{\mathrm{SCF}}) \mathcal{P}_{sig-\mathrm{TM},i} + \overline{f}_{\mathrm{SCF}} \mathcal{P}_{sig-\mathrm{SCF},i} \right] \\
& + N_{q\bar{q}} \frac{1}{2} \left(1 + q_{\mathrm{K},i} A_{q\bar{q}}\right) \mathcal{P}_{q\bar{q},i} \\
& + \sum_{j=1}^{N_{\mathrm{classes}}^{B^+}} N_{B^+}^j \frac{1}{2} \left(1 + q_{\mathrm{K},i} A_{B^+}^j\right) \mathcal{P}_{B^+,i}^j
\end{aligned}$$

$$+ \sum_{j=1}^{N^{B^0}_{\rm classes}} N^j_{B^0} \frac{1}{2} \left(1 + q_{{\rm K},i} A^j_{B^0}\right) \mathcal{P}^j_{B^0,i} \Bigg\} , \quad (15)$$

where,

- N' is the sum of all the yields involved, *i.e.*, $N_{sig} + N_{q\bar{q}} + \sum_{j=1}^{N^{B^+}_{\rm classes}} N^j_{B^+} + \sum_{j=1}^{N^{B^0}_{\rm classes}} N^j_{B^0}$;
- N_{sig} is the total number of signal events in the data sample to be determined in the fit;
- $\overline{f}_{\rm SCF}$ is the fraction of the misreconstructed signal events averaged over the Dalitz plot, which is determined from the fit;
- $\mathcal{P}_{sig-{\rm TM},i}$ and $\mathcal{P}_{sig-{\rm SCF},i}$ are the products of discriminating variable PDFs, for the correctly reconstructed and the misreconstructed signal events, respectively;
- $N_{q\bar{q}}$ is the number of the continuum events, which is determined in the fit;
- $q_{{\rm K},i}$ is the kaon charge of the event; we use $q_{\rm K} = 1$ for B^0 and $q_{\rm K} = -1$ for $\overline{B}^0$;
- $A_{q\bar{q}}$ parameterizes possible charge asymmetry in the continuum events due to detection, reconstruction or selection; it is free in the fit;
- $\mathcal{P}_{q\bar{q},i}$ is the PDF for the continuum events;
- $N^{B^+}_{\rm classes}$ ($N^{B^0}_{\rm classes}$) is the number of the charged (neutral) B-related background classes considered, equal to 6 (4);
- $N^j_{B^+}$ ($N^j_{B^0}$) is the number of events in the charged (neutral) B-related background class j; it is fixed to the MC estimate unless stated otherwise;
- $A^j_{B^+}$ ($A^j_{B^0}$) describes the charge asymmetry in the charged (neutral) B background of class j; this eventual charge asymmetry could come from physics, or detection effects; it is fixed in the fit;
- $\mathcal{P}^j_{B^+,i}$ is the B^+-background PDF for class j;
- $\mathcal{P}^j_{B^0,i}$ is the B^0-background PDF for class j; two dedicated classes are used for $B^0 \to \overline{D}^0\pi^0$, $\overline{D}^0 \to K^+\pi^-$ and $B^0 \to D^-K^+$, $D^- \to \pi^-\pi^0$.

Each PDF $\mathcal{P}_X$ is a product of the PDFs of the four discriminating variables, *i.e.* $\mathcal{P}_{X,i} \equiv P_{X,i}(m_{\rm ES}) \cdot P_{X,i}(\Delta E') \cdot P_{X,i}(s_{+-}, s_{-0})$.

The $m_{\rm ES}$ distribution for the correctly reconstructed signal events is parameterized using a Crystal Ball function [13], the mean and width being simultaneously determined from the fit to data. A sum of two Gaussians is used to describe the $\Delta E'$ distribution, the means, widths and fractions being parameterized as linear functions of the Dalitz plot variable $m^2(K^+\pi^-)$, the intercepts and slopes of which are obtained from simulation, and are varied for systematic uncertainty studies. For the misreconstructed signal, the $m_{\rm ES}$ and $\Delta E'$ distributions are both obtained from simulation.

For the continuum events, the $m_{\rm ES}$ distribution is described by an ARGUS shape function [14] and its $\Delta E'$ distribution is modeled by a linear function. The shape parameter ξ of the ARGUS distribution and the slope of the linear function are determined in a fit to the on-resonance data but

selected with $m_{\rm ES} > 5.23\,{\rm GeV}/c^2$. This dedicated fit uses only $m_{\rm ES}$ and $\Delta E'$ as the discriminating variables, and considers the signal, the continuum background, and the B-backgrounds in a similar way as the nominal fit.

The background class $B^0 \to \overline{D}^0\pi^0\,, \overline{D}^0 \to K^+\pi^-$ shares the parameterizations of $m_{\rm ES}$ and $\Delta E'$ for the signal events. Its yield is determined in the fit to measure the branching fraction.

The shapes of the other B background $m_{\rm ES}$ - $\Delta E'$ PDFs are obtained from MC simulation and parameterized using two-dimensional empirical shape-fitting techniques [15].

The Dalitz plot PDFs for TM and SCF signal events are

$$P_{{\rm TM},i} \;=\; \varepsilon_i\,(1-f_{{\rm SCF},i})\,\frac{|\mathcal{A}_{B^0\to K^+\pi^-\pi^0}|^2 + |\overline{\mathcal{A}}_{\overline{B}^0\to K^-\pi^+\pi^0}|^2}{\mathcal{N}_{\rm TM}}\;, \tag{16}$$

$$P_{{\rm SCF},\,i} \;=\; \varepsilon_i\,f_{{\rm SCF},i}\,\frac{|\mathcal{A}_{B^0\to K^+\pi^-\pi^0}|^2 + |\overline{\mathcal{A}}_{\overline{B}^0\to K^-\pi^+\pi^0}|^2}{\mathcal{N}_{\rm SCF}}\;, \tag{17}$$

where $\mathcal{N}_{\rm TM}$ and $\mathcal{N}_{\rm SCF}$ are the normalization constants to be dynamically determined in the fit, ε_i and $f_{{\rm SCF},i}$ are the efficiency and the misreconstruction fraction, respectively, that vary across the Dalitz plot and are obtained with phase-space MC simulation. The magnitudes and the relative phases in Eq. 4 are fit parameters and are allowed to vary in the fit, except that we fix a_i to 1.0 and both the phases to 0 for the ρ component, since this analysis is only sensitive to relative magnitudes and phases. The masses and widths for intermediate resonances are fixed in the fit and are varied by their uncertainties to estimate the systematic uncertainties in our results. Because the considered intermediate resonances are in general very broad compared to the Dalitz plot resolution, we ignore the resolution effect for the correctly reconstructed signal, while we apply a resolution function (matrix) for the sizable misreconstructed signal.

The Dalitz plot PDF for the continuum events is obtained from the on-resonance sideband events selected with $5.20 < m_{\rm ES} < 5.25\,{\rm GeV}/c^2$, plus the off-resonance events selected with $m_{\rm ES} > 5.20\,{\rm GeV}/c^2$, and is corrected for the expected B-background feed-through in the sideband of $5.20 < m_{\rm ES} < 5.25\,{\rm GeV}/c^2$.

For the background class $B^0 \to \overline{D}^0\pi^0\,, \overline{D}^0 \to K^+\pi^-$, we distinguish the correctly reconstructed events and the misreconstructed events. For the correctly reconstructed events, a single Gaussian is used for the reconstructed D^0 mass distribution, the mean and width being free in the fit, and an empirical $5th$-order polynomial is used to account for the reconstruction efficiency effects for the reconstructed D^0 helicity distribution. For the misreconstructed events, a smoothed two-dimensional histogram is used to parameterize their contributions in the Dalitz plot, which are fixed to the MC expectation. For the other nine classes of B-background, we model their contributions in the Dalitz plot with smoothed histograms obtained from simulation.

Multiple solutions occur in the fit for this Dalitz analysis. To study the effect, we randomize the initial values of the amplitudes and phases that are let free in the fit and then the fit is redone many times. We do observe that there are two sets of solutions that correspond to two log-likelihood ($\log\mathcal{L}$) values. The two $\log\mathcal{L}$ values differ by 0.4 units. Parameters from the two solutions usually give very close values except for the phases of $K^*(892)^0$ and $K_0^*(1430)^0$. Our strategy is to choose the fit that gives the largest likelihood to obtain our nominal results. We also report the other solution for the phases of $K^*(892)^0$ and $K_0^*(1430)^0$.

4 SYSTEMATIC STUDIES

The systematic errors in the branching fractions and CP-violating charge asymmetries, due to assumptions about the decay dynamics, are referred to as "model systematic uncertainty". They are obtained by varying the resonance parameters within their uncertainties, and by adding less significant resonances to the nominal model.

The other systematic errors in the branching fractions are obtained by adding in quadrature those evaluated for the signal yield, the systematic uncertainties in efficiencies of tracking, particle identification, π^0 reconstruction and those corresponding to other selection criteria. The other systematic errors in the A_{CP} measurements are introduced by the uncertainties in the treatment of the B background and by possible charge biases of the detector.

The systematic uncertainties in the signal yield are primarily due to the modeling of the signal, of the B-background, and of the continuum in the ML fit. These are estimated by varying the parameters that are fixed in the nominal fit, within their uncertainties. The variations in the signal yield are added in quadrature. The parameters for the signal $\Delta E'$ PDF are allowed to vary in the fit to the data to estimate the corresponding systematic uncertainty. The expected yields from the background modes are varied according to the uncertainties in the measured or estimated branching fractions. Biases observed in toy MC fits are added in quadrature and assigned as a systematic uncertainty of the fit procedure, referred to as "fitting procedure" in Table 2.

The basis for evaluating the systematic uncertainties on the cuts that are applied in the selection process is to study the differences in $m_{\rm ES}$, $\Delta E'$ and the NN output between on-resonance data and Monte Carlo simulation. The corrections and uncertainties in the signal efficiencies are summarized in Table 2. The parameters for the signal $m_{\rm ES}$ and $\Delta E'$ PDFs are obtained from the fit to the data and are used to estimate the systematic errors due to the cuts on $m_{\rm ES}$ and $\Delta E'$, respectively. The difference between the data and Monte Carlo distributions of the NN output is extracted from fully-reconstructed $B^+ \to K^+\pi^-\pi^0\pi^+$ decays via intermediate D^0 or D^*, and is used to estimate the systematic error due to the cut on the NN output.

Since B background modes may exhibit direct CP violation, the corresponding parameters (the A_B^j's in Eq. 15) are varied by ± 0.5 to conservatively estimate the uncertainties.

Table 2 summarizes the various sources contributing to the systematic errors in the branching fractions. The dominant systematic errors are due to the π^0 resonstruction, the $\Delta E'$ cut, and the cut on the NN output. Table 3 summarizes the possible sources contributing to the systematic errors in the charge asymmetries.

5 RESULTS

The preliminary results are obtained with a fit to the data sample using our nominal model. We obtain 1230 ± 74 signal events and 454 ± 24 $B^0 \to \overline{D}^0\pi^0, \overline{D}^0 \to K^+\pi^-$ events from the data sample. The results obtained with the nominal model are shown in Table 4. The total sum of the fractions obtained with the nominal fit is $(102.6 \pm 8.0)\%$. Table 5 shows the results for the less significant modes, obtained by adding in turn one mode to the nominal fit. The results obtained from these altered fits, for the modes in the nominal model, are compatible.

The inclusive signal efficiency is estimated to be $(16.6 \pm 0.1)\%$ with the observed Dalitz plot structure. We measure the inclusive branching fraction to be:

$$\mathcal{B}(B^0 \to K^+\pi^-\pi^0) \;=\; (34.9 \pm 2.1(stat.) \pm 3.9(syst.)) \times 10^{-6}\,. \tag{18}$$

Table 2: Breakdown of systematic errors for the branching fraction measurements. The error from each source varies slightly for each intermediate state and the most conservative estimate is quoted.

	Charmless yield (events)	$\overline{D}^0\pi^0$ yield (events)
Continuum $m_{\rm ES}$ PDF	4.3	0.0
Continuum $\Delta E'$ PDF	2.0	0.0
Signal $\Delta E'$ PDF	50.0	12.4
B backgrounds	2.7	11.2
Fitting procedure	22.7	0.0
Sub-total (relative)	55.2 (4.5%)	16.7 (3.7%)
	Efficiency and scaling systematics (relative)	
Tracking efficiency correction	1.6%	
PID for tracks	2.0%	
π^0 reconstruction	6.4%	
ΔE cut efficiency	4.6%	
m_{ES} cut efficiency	0.4%	
NN cut efficiency	6.0%	
N($B\overline{B}$)	1.1%	
Sub-total	10.3%	
Total systematic error	11.2%	10.9%

Table 3: Breakdown of systematic errors for the A_{CP} measurements.

	$K^*(892)^+$	$\rho(770)^-$	$K_0^*(1430)^+$	$K_0^*(1430)^0$	$K^*(892)^0$	NR
Detector bias			0.01			
B backgrounds	0.02	0.04	0.06	0.07	0.07	0.20
Total systematic error	0.02	0.04	0.06	0.07	0.07	0.20

We find

$$\mathcal{B}(B^0 \to \overline{D}^0\pi^0) \;=\; (3.3 \pm 0.2(stat.) \pm 0.4(syst.)) \times 10^{-4}\,. \tag{19}$$

The signal significance for $\mathcal{B}(B^0 \to K^*(892)^0\pi^0)$, including statistical and systematic errors, is 4.2σ. We set an upper limit of $\mathcal{B}(B^0 \to K^+\pi^-\pi^0\ nonresonant) < 4.7 \times 10^{-6}$ at 90% confidence level, with systematic errors being taken into account.

There exists another solution with a $\log\mathcal{L}$ 0.4 units lower than the maximum $\log\mathcal{L}$. This solution gives very compatible results except for the relative phases of $K_0^*(1430)^0$ and $K^*(892)^0$.

The Dalitz plot for the selected $K^+\pi^-\pi^0$ events is shown in Fig. 1. The $m_{\rm ES}$ and $\Delta E'$ projections are shown in Fig. 2. Projection plots of the invariant mass pairs are shown in Fig. 3.

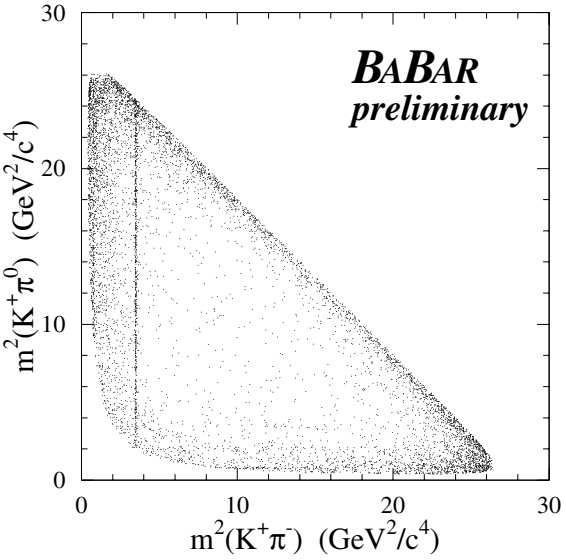

Figure 1: Dalitz plot for the selected $K^+\pi^-\pi^0$ events. The visible narrow band comes from the $B^0 \to \overline{D}^0\pi^0$ decays.

6 SUMMARY

Due to lack of knowledge of the final state interactions in $B \to K^+\pi^-\pi^0$ decays, this Dalitz analysis assumes uniform phase space for the nonresonant decay amplitude and utilizes parameterizations obtained from non-B-meson experiments to model the intermediate resonant amplitudes. Non-unique parameterizations of the decay amplitude are covered by the systematic uncertainties.

A comparison with other measurements is summarized in Table 6.

The measured branching fraction of $B^0 \to \overline{D}^0\pi^0$ is in good agreement with the current world average, $(2.7 \pm 0.8) \times 10^{-4}$ [9].

The measured branching fractions and charge asymmetries of the decays $B^0 \to \rho(770)^- K^+$ and $B^0 \to K^*(892)^+\pi^-$ are in agreement with the previously reported measurements [4, 5, 6].

We report observations of the intermediate S-wave decays, $B^0 \to K_0^*(1430)^+\pi^-$ and $B^0 \to K_0^*(1430)^0\pi^0$, with the LASS parameterization [12]. We do not see any significant direct CP

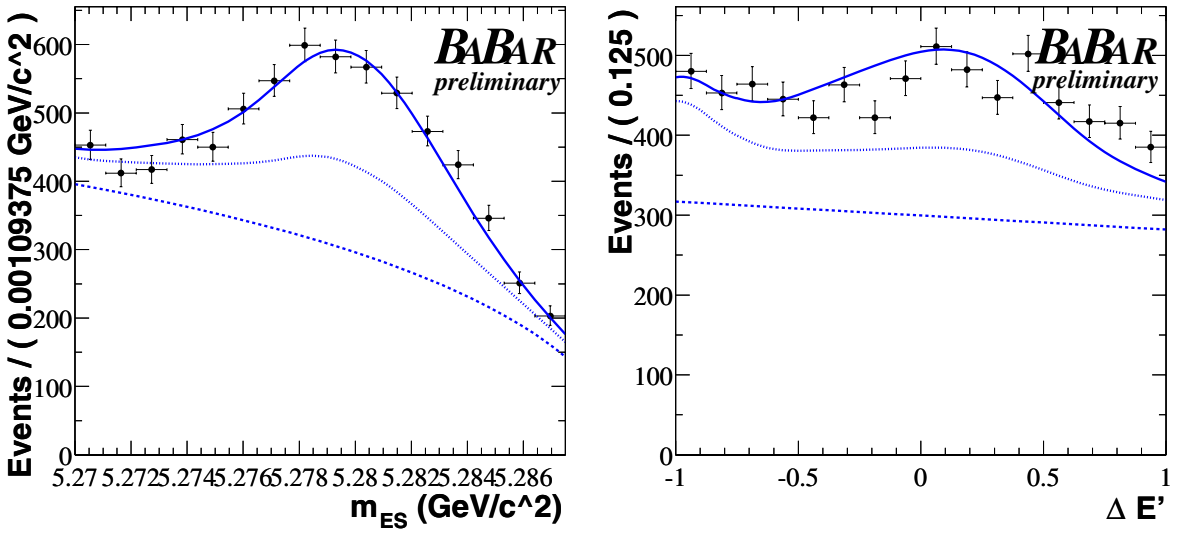

Figure 2: $m_{\rm ES}$ (left) and $\Delta E'$ (right) projections for the selected $K^+\pi^-\pi^0$ events. The data are the points with error bars. The fit result is the (top) solid line. The (bottom) dashed line represents the continuum background and the (middle) dotted line is the B background added on top of the continuum background. Note that the B backgound includes the $B^0 \to \overline{D}^0\pi^0$, $\overline{D}^0 \to K^+\pi^-$decays.

violation in these two decay modes.

We observe the first evidence of $B^0 \to K^*(892)^0\pi^0$ decay with a branching fraction in agreement with the reported upper limit [6]. We do not see any direct CP violation in this decay mode.

We set upper limits on the branching fractions of the nonresonant decay and the other six less significant intermediate states.

7 ACKNOWLEDGMENTS

We are grateful for the extraordinary contributions of our PEP-II colleagues in achieving the excellent luminosity and machine conditions that have made this work possible. The success of this project also relies critically on the expertise and dedication of the computing organizations that support *BABAR*. The collaborating institutions wish to thank SLAC for its support and the kind hospitality extended to them. This work is supported by the US Department of Energy and National Science Foundation, the Natural Sciences and Engineering Research Council (Canada), Institute of High Energy Physics (China), the Commissariat à l'Energie Atomique and Institut National de Physique Nucléaire et de Physique des Particules (France), the Bundesministerium für Bildung und Forschung and Deutsche Forschungsgemeinschaft (Germany), the Istituto Nazionale di Fisica Nucleare (Italy), the Foundation for Fundamental Research on Matter (The Netherlands), the Research Council of Norway, the Ministry of Science and Technology of the Russian Federation, and the Particle Physics and Astronomy Research Council (United Kingdom). Individuals have received support from CONACyT (Mexico), the A. P. Sloan Foundation, the Research Corporation, and the Alexander von Humboldt Foundation.

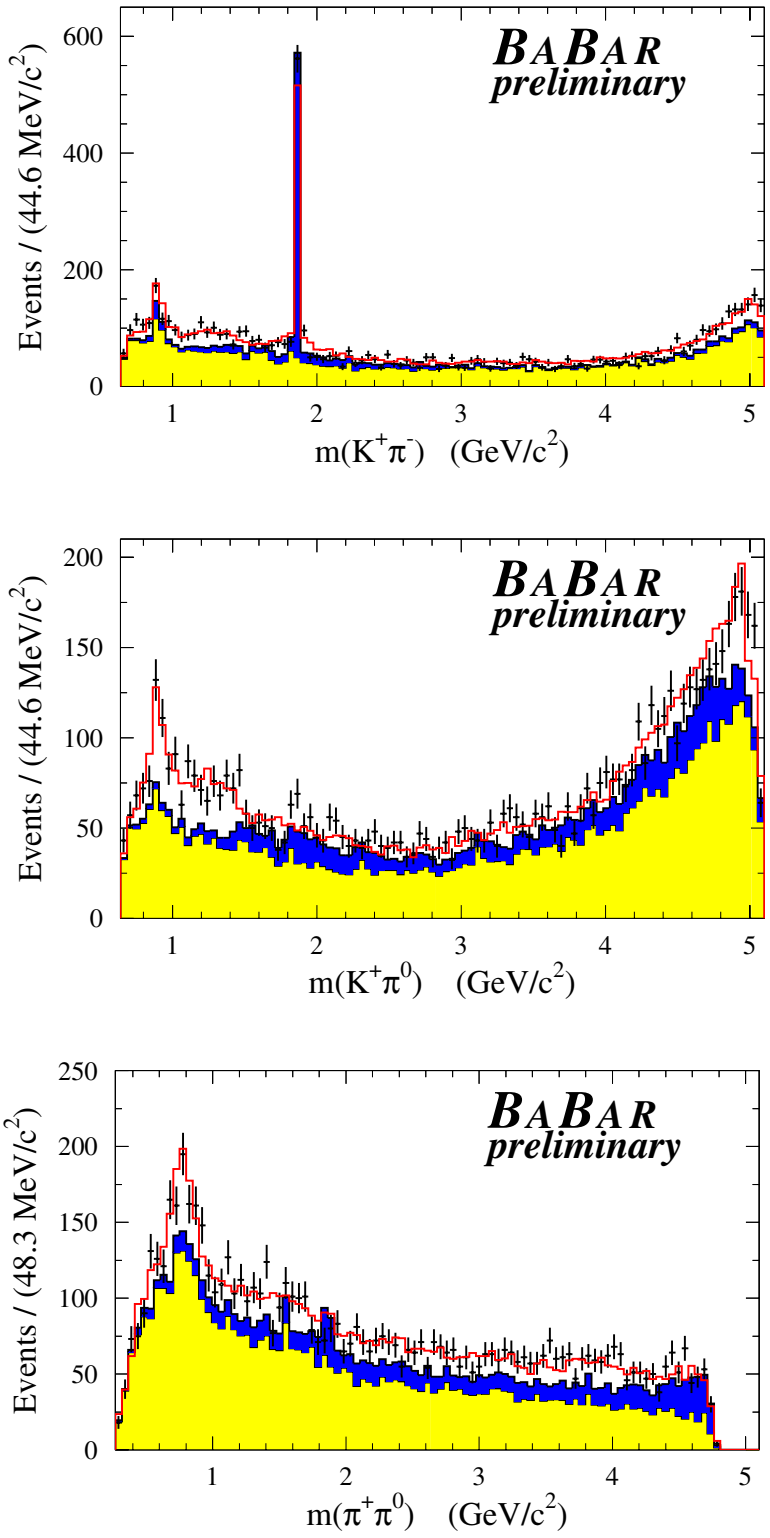

Figure 3: Projection plots for the mass pairs. The data are the black points with error bars (statistical only). The total fit result is the solid (red) line. The continuum background is the light shaded (yellow) and the B-background is the dark shaded (blue) added on top of the continuum background.

Table 4: Results obtained with a fit to the data using the nominal model. The first errors in the table are statistical while the second and the third (when present) are systematic errors as discussed in Sec. 4. The last column indicates the likelihood change when the mode is omitted in turn in the nominal model. f and A_{CP} have been defined in Eq. 12, while ϕ and $\overline{\phi}$ have been defined in Eq. 4. For the other solution, $\phi_{K_0^*(1430)^0} = (106 \pm 44)^\circ$, $\phi_{K^*(892)^0} = (-44 \pm 48)^\circ$, and all the other parameters give very compatible results.

Mode	f (%)	ϕ / $\overline{\phi}$ (degree)	A_{CP}	$\Delta \log \mathcal{L}$
$K^*(892)^+\pi^-$	$10.4^{+2.1}_{-2.0} \pm 0.8$	138 ± 35 / 174 ± 42	$-0.25 \pm 0.17 \pm 0.02 \pm 0.02$	-42.5
$\rho(770)^- K^+$	$24.6^{+3.6}_{-2.9} \pm 0.6$	0.0 (fixed) / 0.0 (fixed)	$0.13^{+0.14}_{-0.17} \pm 0.04 \pm 0.13$	-48.3
$K_0^*(1430)^+\pi^-$	$32.2 \pm 3.8 \pm 9.4$	115 ± 34 / 149 ± 35	$-0.07 \pm 0.12 \pm 0.06 \pm 0.05$	-92.9
$K_0^*(1430)^0\pi^0$	$22.5 \pm 4.0 \pm 7.2$	-12 ± 40 / 8 ± 42	$-0.34 \pm 0.15 \pm 0.07 \pm 0.08$	-71.4
$K^*(892)^0\pi^0$	$5.8^{+1.7}_{-1.5} \pm 0.6$	-160 ± 41 / -144 ± 41	$-0.01^{+0.24}_{-0.22} \pm 0.07 \pm 0.11$	-23.8
$Nonresonant$	$7.1^{+3.6}_{-2.9} \pm 0.1$	55 ± 28 / 79 ± 28	$-0.12^{+0.36}_{-0.37} \pm 0.20 \pm 0.07$	-7.3

Table 5: Results obtained for the less significant intermediate states when they are added to the nominal model in turn. The last column indicates the likelihood change.

Mode	Fraction (%)	$\Delta \log \mathcal{L}$
$K_2^*(1430)^+\pi^-$	$3.5^{+2.0}_{-1.5}$	7.3
$K_2^*(1430)^0\pi^0$	$1.6^{+1.7}_{-1.4}$	3.4
$K^*(1680)^+\pi^-$	$3.9^{+2.3}_{-1.7}$	5.8
$K^*(1680)^0\pi^0$	$0.8^{+1.4}_{-0.8}$	1.6
$\rho(1450)^- K^+$	$5.0^{+2.8}_{-2.7}$	3.6
$\rho(1700)^- K^+$	$2.5^{+1.8}_{-1.5}$	2.1

References

[1] N. Cabibbo, Phys. Rev. Lett. **10**, 531 (1963); M. Kobayashi, T. Maskawa, Prog. Theor. Phys. **49**, 652 (1973).

Table 6: Comparison between measurements of branching fractions ($\times 10^{-6}$) and CP-violating charge asymmetries. Note that Belle measured K^*_X, which is defined to have $1.1\,\mathrm{GeV}/c^2 < m(K^+\pi^{-,0}) < 1.6\,\mathrm{GeV}/c^2$ and has a helicity angular distribution indicating a scalar behavior. Our preliminary results in this table are corrected for the secondary decay branching fractions except for those indicated by a †. Previously published results from *BABAR* on $\rho^- K^+$ (listed within parentheses) were obtained with a subset of 81 fb^{-1} of the data used for this analysis.

	CLEO	Belle	*BABAR*
$\mathcal{B}(B^0 \to K^+\pi^-\pi^0$ inclusive)	< 40	$36.6 \pm 4.2 \pm 3.0$	$34.9 \pm 2.1 \pm 3.9$
$A_{\rm CP}(B^0 \to K^+\pi^-\pi^0$ inclusive)	-	$0.07 \pm 0.11 \pm 0.01$	-
$\mathcal{B}(B^0 \to K^*(892)^+\pi^-)$	$16 \pm 6 \pm 2$	$14.8 \pm 4.6 \pm 1.5 \pm 2.4$	$10.9 \pm 2.3 \pm 1.5$
$A_{\rm CP}(B^0 \to K^*(892)^+\pi^-)$	$0.26^{+0.33+0.19}_{-0.34-0.08}$	-	$-0.23 \pm 0.17 \pm 0.02 \pm 0.02$
$\mathcal{B}(B^0 \to K^*(892)^0\pi^0)$	< 3.6	< 3.5	$3.0 \pm 0.9 \pm 0.5$
$A_{\rm CP}(B^0 \to K^*(892)^0\pi^0)$	-	-	$-0.01^{+0.24}_{-0.22} \pm 0.07 \pm 0.11$
$\mathcal{B}(B^0 \to \rho(770)^- K^+)$	$16 \pm 8 \pm 3$	$15.1 \pm 3.4 \pm 1.5 \pm 2.1$	$8.6 \pm 1.4 \pm 1.0$
$A_{\rm CP}(B^0 \to \rho(770)^- K^+)$	-	$0.22^{+0.22+0.06}_{-0.23-0.02}$	$(7.3 \pm 1.3 \pm 1.3)$ $0.13^{+0.14}_{-0.17} \pm 0.04 \pm 0.13$ $(0.18 \pm 0.12 \pm 0.02)$
$\mathcal{B}(B^0 \to K_0^*(1430)^0\pi^0)^\dagger$	-	$6.1^{+1.6+0.5}_{-1.5-0.6}$	$7.9 \pm 1.5 \pm 2.7$
$A_{\rm CP}(B^0 \to K_0^*(1430)^0\pi^0)$	-	-	$-0.34 \pm 0.15 \pm 0.07 \pm 0.08$
$\mathcal{B}(B^0 \to K_0^*(1430)^+\pi^-)^\dagger$	-	$5.1 \pm 1.5^{+0.6}_{-0.7}$	$11.2 \pm 1.5 \pm 3.5$
$A_{\rm CP}(B^0 \to K_0^*(1430)^+\pi^-)$	-	-	$-0.07 \pm 0.12 \pm 0.06 \pm 0.05$
$\mathcal{B}(B^0 \to K^+\pi^-\pi^0$ NR)	-	< 9.4	< 4.6
$\mathcal{B}(B^0 \to K_2^*(1430)^+\pi^-)^\dagger$	-	-	< 2.2
$\mathcal{B}(B^0 \to K_2^*(1430)^0\pi^0)^\dagger$	-	-	< 1.2
$\mathcal{B}(B^0 \to K^*(1680)^+\pi^-)^\dagger$	-	-	< 2.5
$\mathcal{B}(B^0 \to K^*(1680)^0\pi^0)^\dagger$	-	-	< 1.3
$\mathcal{B}(B^0 \to \rho(1450)^- K^+)^\dagger$	-	-	< 3.2
$\mathcal{B}(B^0 \to \rho(1700)^- K^+)^\dagger$	-	-	< 1.7

[2] C.W. Chiang, M. Gronau, Z.L. Luo, J.L. Rosner, D.A Suprun, Phys. Rev. **D69**, 034001(2004).

[3] N.G. Deshpande and X. He, Phys. Rev. Lett. **74**, 26 (1995);
R. Fleisher, Z. Phys. **C62**, 81 (1994).

[4] CLEO Collaboration, E. Eckhart *et al.*, Phys. Rev. Lett. **89**, 251801 (2002).

[5] *BABAR* Collaboration, B. Aubert *et al.*, Phys. Rev. Lett. **91**, 201802 (2003).

[6] Belle Collaboration, P. Chang *et al.*, BELLE-CONF-0317, hep-ex/0406075 (2003).

[7] *BABAR* Collaboration, B. Aubert *et al.*, Nucl. Instrum. Methods **A479**, 1-116 (2002).

[8] J. Blatt and V. Weisskopf, *"Theoretical Nuclear Physics"*, John Wiley & Sons, New York, 1956.

[9] Particle Data Group, S. Eidelman *et al.*, Phys. Lett. **B592**, 1 (2004).

[10] G.J. Gounaris and J.J. Sakurai, Phys. Rev. Lett. **21**, 244 (1968).

[11] P. Estabrooks, Phys. Rev. **D19**, 2678 (1979).

[12] D. Aston *et al.*, Nucl. Phys. **B296**, 493 (1988).

[13] J.E. Gaiser *et al.*, Phys. Rev. **D34**, 711 (1986).

[14] ARGUS Collaboration, H. Albrecht *et al.*, Z. Phys. **C48**, 543 (1990).

[15] K.S. Cranmer, Comput. Phys. Commun. **136**, 198 (2001), hep-ex/0011057, ALEPH 99-144 (1999).